Carbon Nanotube Reinforced *Bombyx mori* Silk Nanofibers by the Electrospinning Process

Jonathan Ayutsede,[†] Milind Gandhi,[‡] Sachiko Sukigara,[§] Haihui Ye,[∥] Chen-ming Hsu,[⊥] Yury Gogotsi,[∥] and Frank Ko*,[†]

Fibrous Materials Laboratory, Department of Materials Science and Engineering, Drexel University, 3141 Chestnut Street, Philadelphia, Pennsylvania 19104, School of Biomedical Engineering, Sciences and Health Systems, Drexel University, Philadelphia, Pennsylvania 19104, Faculty of Education and Human Sciences, Niigata University, Japan, A. J. Drexel Nanotechnology Institute and Department of Materials Science and Engineering, Drexel University, Philadelphia, Pennsylvania 19104, and Taiwan Textile Research Institute, Taiwan

Received August 17, 2005; Revised Manuscript Received October 20, 2005

Nanocomposite fibers of *Bombyx mori* silk and single wall carbon nanotubes (SWNT) were produced by the electrospinning process. Regenerated silk fibroin dissolved in a dispersion of carbon nanotubes in formic acid was electrospun into nanofibers. The morphology, structure, and mechanical properties of the electrospun nanofibers were examined by field emission environmental scanning electron microscopy (SEM), transmission electron microscopy (TEM), Fourier transform infrared (FTIR) spectroscopy, Raman spectroscopy, and microtensile testing. TEM of the reinforced fibers shows that the single wall carbon nanotubes are embedded in the fibers. The mechanical properties of the SWNT reinforced fiber show an increase in Young's modulus up to 460% in comparison with the un-reinforced aligned fiber, but at the expense of the strength and strain to failure.

Introduction

Protein-based polymers with good biocompatibility and structural properties such as silk have been used as suture and textile materials.[1] The triangular cross section and 10−20 μm size of *Bombyx mori* fibers remain unchanged over the years. The fibers consist of thousands of parallel fibrils which give them their grainy surfaces. This paper examines the scientific implications of reducing the fiber diameter to the nanoscale, changing the triangular cross section of the fiber and reinforcing the fibers with SWNT by the electrospinning process. We envision new tailorable properties for the nanofibers such as reduction in static electricity, higher tensile modulus and strength.

Electrospinning is an attractive method of producing nanoscale fibers from natural[2] and synthetic sources[3] with diameters ranging from 2 nm to several micrometers. Fiber diameters as low as 7 nm with near circular cross section, smooth surfaces and improved biocompatibility can be produced by electrospinning regenerated silk fibroin devoid of sericin.[4−7] However, the mechanical properties of the electrospun silk fiber[8,9] were lacking in comparison with the natural fiber. This could be due to the fact that the electrospun fibers were tested in yarns or nonwoven mats, which do not give accurate values of the nanofiber properties. The discrepancy in mechanical properties of the electrospun and natural silk fiber may also be as a result of the processing steps involved in the nanofiber formation, differences in crystallinity, and molecular orientation of the chains along the fiber axis. Experiments have shown that electrospinning of nanofibers does indeed lead to a certain degree of molecular orientation of the chains that comprise the fibers;[10−12] however, some of this orientation is lost due to relaxation processes that occur immediately after fiber formation. Drawing of fibers is one of the postprocessing methods for improving the mechanical properties due to improvement of the degree of molecular orientation. Vollrath et al. have shown that it's possible to attain silkworm silk fibers with improved mechanical properties by drawing[13] and artificial reeling of silk straight from the silkworm at high speeds (27 mm/s).[14]

There is therefore a need to improve on the mechanical properties of the electrospun silk fibers. The availability of SWNT which have exceptional mechanical (elastic modulus and tensile strength of 1TPa and 200 GPa respectively)[15] and electrical properties make them suitable candidates for tailoring not only the mechanical properties of a material but also may elicit changes in the electrical and thermal properties. Thus, SWNT's have potential applications as polymer reinforcements for composites, materials for energy storage,[16] electronics,[17] catalysis,[18] and vaccine delivery.[19]

Utilizing SWNTs will provide design options of tailoring the mechanical properties of polymers for various applications such as in tissue engineering for the fabrication of cell-growth scaffolds[20,21] and vascular grafts.[22,23] The improved mechanical properties of the SWNT-reinforced nanofibers may have an effect on the transfer of mechanical stimuli to the cells. An enormous reinforcement effect with the use of only a small portion of SWNT can be anticipated. However, the challenges involved in the fabrication of SWNT reinforced polymers such as homogeneous dispersion of the SWNTs in the polymer, efficient load transfer, aggregation and poor solubility in water and organic solvents, acts as limitations for practical applica-

* To whom correspondence should be addressed. E-mail: fko@coe.drexel.edu. Tel: (215) 895-1640. Fax: (215) 895-6684.

[†] Fibrous Materials Laboratory, Department of Materials Science and Engineering, Drexel University.

[‡] School of Biomedical Engineering, Sciences and Health Systems, Drexel University.

[§] Niigata University.

[∥] A. J. Drexel Nanotechnology Institute and Department of Materials Science and Engineering, Drexel University.

[⊥] Taiwan Textile Research Institute.

10.1021/bm0505888 CCC: $33.50
Published on Web 12/16/2005

tions. Many strategies have been employed to separate and disperse the SWNTs which include sonication,[24] covalent[25] and ionic functionalization,[26,27] and steric[28] and electrostatic repulsion.[29]

In recent years, SWNTs have been utilized as nanofillers to enhance the mechanical properties of polymeric materials.[30−32] Andrews et al. dispersed SWNT's in isotropic petroleum pitch matrixes to form nanotube composite carbon fibers with enhanced mechanical and electrical properties[33] (5 wt % loading of SWNT's led to an increase in modulus by 150%). Ko et al. fabricated carbon nanotube-polyacrylonitrile composite fibers by the electrospinning process.[34,35] They utilized both SWNT's and multiwall carbon nanotubes and studied the reinforcement effects of the nanotubes on the nanofibers. A two-stage rupture behavior of the composite fibers under tension, including crazing of polymer matrix and pull-out of carbon nanotubes was observed. They concluded that carbon nanotubes reinforce the polymer fibers by hindering crazing extension, reducing stress concentration, and dissipating energy by pullout.

To date, to our knowledge, no one has studied the reinforcement effects of SWNTs on natural biopolymers. Spider silk is known as the toughest natural material; however, efforts to produce it on a commercial scale have not been successful. On the other hand, natural silkworm silk, which is produced on a large commercial scale, without postprocessing treatments, usually lacks the toughness and strength of spider silk. We hypothesize that by reinforcing the silk fibers with SWNT's, a significant improvement may be made in its mechanical properties. We propose using the silk fibroin as the dispersing agent for the SWNT's with a net gain effect of having the electrospun nanofibers reinforced by the latter. The dispersion should be driven by both steric and hydrophobic effects between silk and SWNT. van der Waals interaction forces also provide cohesion between the SWNTs and silk. The rigidity and cylindrical shape of SWNTs make their surfaces good supports for protein crystallization[36] which can improve the mechanical properties of the electrospun nanofibers. Consequently, by co-electrospinning SWNT with silk fibroin, a nanocomposite fiber may be fabricated to yield multifunctional strong and tough fibers, which may open the gateway to producing multifunctional fibers that may be suitable for weaving into textiles.

Here, we report the reinforcement effects of SWNT's on the morphology, structure and mechanical properties of electrospun silk nanofibers.

Experimental Section

Degummed *Bombyx mori* silk fibers provided by the Taiwan Textile Research Institute were dissolved in 50% aqueous calcium chloride ($CaCl_2$) and dialyzed against deionized water for 2−3 days. The dialyzed fibroin solution was frozen for 24 h at −20 °C and then lyophilized at −80 °C (LabConco Freezone 2.5 Plus) to produce sponges. Purified SWNTs produced by high-pressure disproportionation of CO (HiPCO)[37] were used. Formic acid and calcium chloride were purchased from Sigma-Aldrich.

The spinning dope was prepared by sonicating 0.5−5 wt % SWNT's in formic acid (98−100%) for 2 h. Regenerated silk fibroin (12 wt %) was added to the SWNT-formic acid mixture and further sonicated for an hour and mechanically stirred for another hour. The SWNT-silk-formic acid solutions were electrospun utilizing an 18-G needle at a 45° spinning angle, a voltage of 30 kV and spinning distance of 7 cm as described in our earlier paper.[38] Random fibers were collected on an aluminum foil covered metallic plate and aligned fibers were collected to make nonwoven mats and yarns, respectively.

The diameter and morphology of the gold-sputtered electrospun SWNT reinforced nanofibers were determined and examined by SEM (Phillips XL-30 field-emission SEM). The average fiber diameter and its distribution were determined based on measuring 100 randomly selected fibers obtained from each spinning condition. The TEM images were obtained using a JEOL-2010F (200 kV) with a point-to-point resolution of 0.23 nm. The samples were prepared by drawing out small fibrils from the silk assemblies (yarns) with the aid of tweezers and placed on lacey carbon coated copper grids.

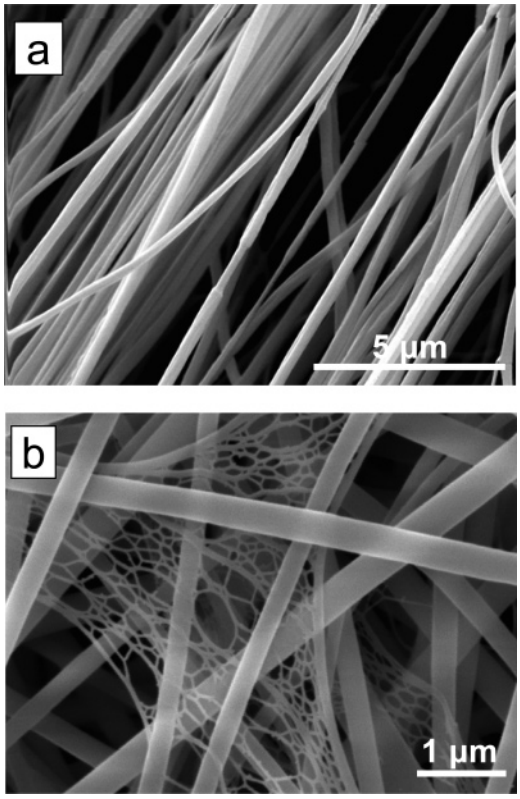

Figure 1. SEM micrographs of 1% SWNT reinforced fibers: (a) aligned and (b) random with a weblike structure.

Raman spectroscopy (Renishaw 1000, 780 nm diode laser), FTIR (Nicolet Magna-IR 560 spectrometer), and wide-angle X-ray diffraction (XDS 2000, Scintag Inc.) were used to elucidate the secondary structure, chemical composition, and crystallinity of the SWNT reinforced fibers. At least 5 spectra were recorded per sample and data are based on averages. The laser spot size and power employed in the Raman measurements were 1 μm and 50−100%, respectively. Deconvolution of the Raman spectra was done by peak fitting application provided by GRAMS-32 software, which uses an iterative fitting of Gaussian functions with the data minimized by the chi-squared criterion. The mechanical properties of the co-electrospun SWNT-silk fibers were measured on the KES-G1 Kawabata microtensile tester at room temperature. A strain rate of 0.02 s^{-1} was used in the tensile tests.

Results and Discussion

The SEM micrographs of electrospun 1 wt % SWNT reinforced fibers (Figure 1) show that the fibers have smooth surfaces. Analysis of the cross sections of the fibers shows that they have near circular cross-sections (not shown). Random structures (nonwoven mat), aligned fibers, and weblike structures can be obtained (Figure 1b). The web formation, as postulated by Gogotsi and Lam,[39] may be a result of the inclusion of carbon nanotubes into the fibers. Due to the methods of dispersion of the SWNTs by sonication and mechanical stirring, the SWNT clusters break down into small ropes. The addition of silk forms a coating around each individual rope and keeps them from aggregating or binding together. During electrospinning, the

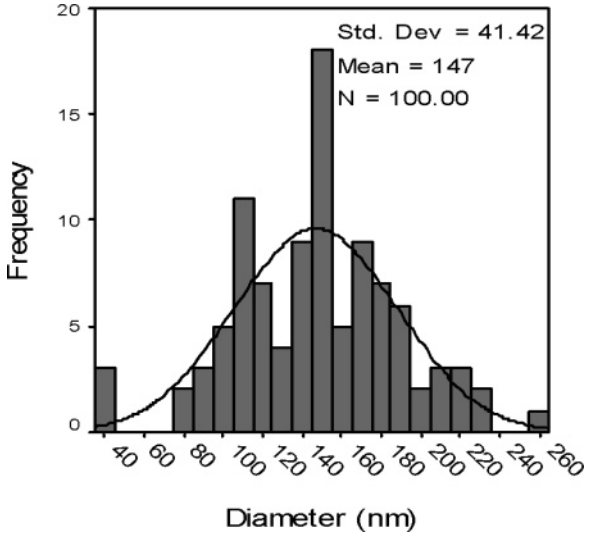

Figure 2. Fiber diameter distribution of 1% SWNT reinforced aligned silk fibers at spinning conditions of 12% silk fibroin concentration, 7 cm spinning distance and electric field of 3 kV/cm.

Table 1. Average Fiber Diameters of SWNT Reinforced Silk Fibers

SWNT content (%)	type of fiber	average diameter (nm)
0.5	random	54 ± 26
0.5	aligned	83 ± 30
1	random	153 ± 99
1	aligned	147 ± 41
2	random	70 ± 33
2	aligned	55 ± 20
5	random	81 ± 33
5	aligned	35 ± 15

bundles are expelled from the polymer jet under extremely high force and velocity, which causes opening of the bundles to form the weblike structure.

Fiber diameter distribution is shown in Figure 2. The average fiber diameter is 147 ± 41 nm. The average fiber diameters for all loadings of SWNT in the silk fibers are all below the 200 nm range as shown in Table 1. There is a general trend of the aligned reinforced fibers of having lower average fiber diameters than their random counterparts. We believe that this is due to the fact that, during the electrospinning and fiber formation process, electrostatic forces stretch the fibers, and upon collection on a plate, the fibers become relaxed and tend to expand in diameter. The aligned fibers on the other hand, were collected between two points under tension and hence their relaxation and expansion values are lower, leading to lower average fiber diameters.

The presence of SWNT in the fibers and the secondary structure of the reinforced silk fibers were determined by Raman spectroscopy. It is also a useful tool for determining the conformation of proteins. Figure 3 shows the spectra of 0.5, 1, 2, and 5% SWNT reinforced aligned fibers with characteristic bands at 1593 and 1570 cm^{-1} (tangential mode [TM]), 195−270 cm^{-1} (radial breathing mode [RBM]), and 1299 cm^{-1} (disorder induced mode [D]) and some minor bands attributed to the silk fibroin. The RBM bands have a diameter-dependent frequency that can be used to determine the nanotubes diameters. The diameters of the SWNT range from 0.84 to 1.13 nm as determined from their RBM bands.[40] The TM band is derived from the in-plane Raman-active mode in graphite and can be

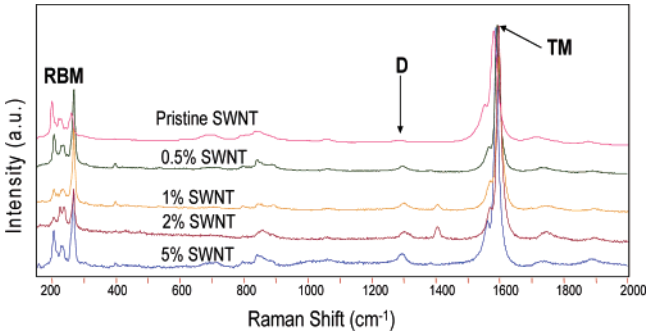

Figure 3. Raman spectra of pristine SWNT and aligned electrospun silk nanofibers with 0.5% to 5% of SWNT.

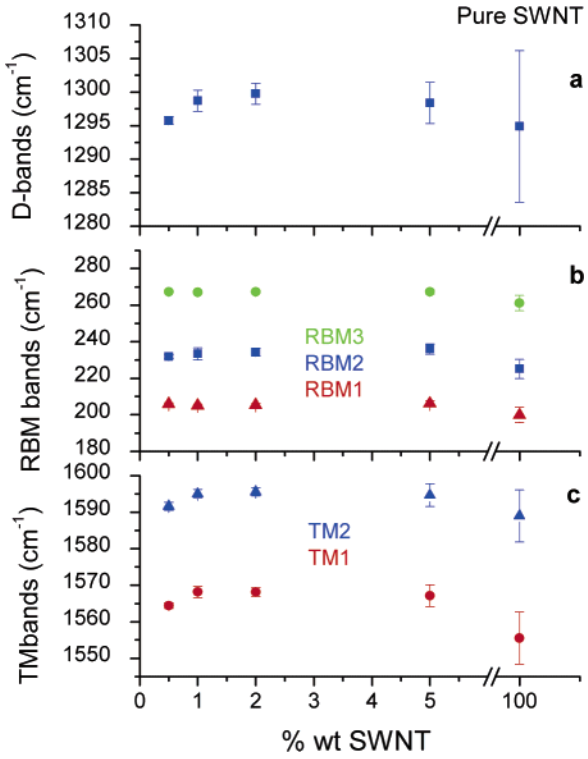

Figure 4. Raman spectroscopy measurements of band positions in SWNT reinforced silk fibers: (a) D-band positions, (b) RBM1-RBM3 band positions, and (c) TM1 and TM2 band positions.

used to differentiate metallic from semiconducting nanotubes. The Raman spectra show that most of the SWNT are semiconducting. The D band on the other hand, originates from double resonance mechanism that couples electrons and phonons.[41] The D band provides information about the crystalline quality of the samples, i.e., disorder and defects in the sp^2 carbon material, and is a useful probe for measuring degrees of structural disorder in the nanotubes.[42]

The D-band occurs in the pristine SWNT at 1294.9 cm^{-1} and can be assigned to defects and tube curvature. It may also originate from small amounts of amorphous carbon remaining on the tube surface after purification, because it was not present in the double-walled nanotubes samples subjected to oxidative cleaning.[43] The D-band positions are dependent on the SWNT incorporation in the silk fiber as shown in Figure 4a. As the concentration of SWNT increases from 0.5%, there is a shift of D-band peak positions to higher frequencies. The D-band increases up to 2% SWNT loading (1299.8 cm^{-1}) after which further increases in the % of SWNT lead to slight decreases in D-band frequency at 5% (1298.4 cm^{-1}). In comparison with the pristine SWNT, there is a downward shift in the D-band by

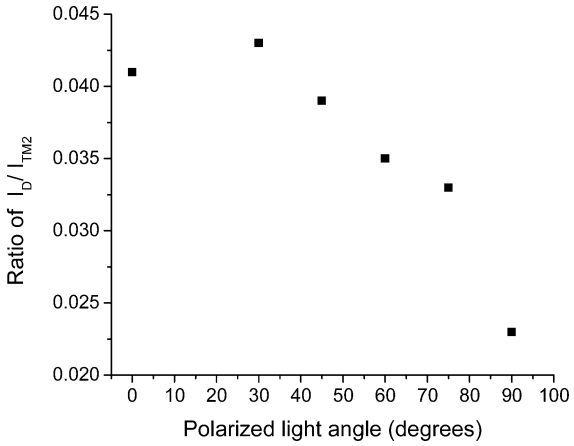

Figure 5. Intensity ratios of D and TM bands in 1% SWNT reinforced silk fiber as function of the orientation of the polarized laser beam relative to the fiber orientation.

4.9 cm^{-1}. It is not clear if the shifts observed in the D-band positions are due to scattering effects.

The RBM peaks shown in Figure 4b occur in the range of 205−267 cm^{-1}. These peaks are attributed to the radial breathing mode of the nanotubes, and its frequency depends on the inverse diameter and on interaction with the surrounding media (silk). The RBM peak positions appear constant when the concentration of SWNT is increased from 0.5 to 5%. The pristine SWNT have somewhat lower RBM values in comparison with the reinforced fibers, which can be attributed to the silk-SWNT interaction. The TM bands shown in Figure 4c also depict similar increases in peak positions as with the D-bands. As the concentration of SWNT increases from 0.5wt %, there is a shift of TM peak positions to higher frequencies. There is an increase up to 1% [1568.2 (TM1) and 1595.0 cm^{-1} (TM2)] after which increasing the loading level of SWNT does not affect the peak position. In comparison with the pristine SWNT, there is an upward shift in the TM1 and TM2 bands by 12.7 and 6.6 cm^{-1}, respectively. Whether these small shifts are related to the interactions between silk and SWNT loadings or as a result of heating of the nanotubes during measurements needs further investigation.

The observed changes in the TM (1595 cm^{-1})-peak intensities of the 0.5−2% SWNT reinforced silk fibers might suggest that the quantity of silk intercalated between the nanotubes increases with increase in SWNT content. As silk is a poor electrical conductor, it may act as an insulator to the nanotubes hence reducing the TM peak intensities. This may lead to better dispersion of the nanotubes and weaker interactions between the nanotubes. For higher concentrations (∼5%), the peak intensities do not change with increase in SWNT content, which may be an indication of saturation of the composite. It seems that higher concentrations of SWNT lead to higher aggregates, which may prevent the silk from being intercalated. Although measured changes on peak positions are very small and may result from data scattering or sample heating with the laser beam, their systematic nature suggests that the observed shift might result from SWNT−polymer interactions.

Polarized Raman spectroscopy was carried out to determine the alignment of the nanotubes in the reinforced fibers. Figure 5 displays the polarized Raman spectra of 1% SWNT-reinforced fibers taken at various angle (θ) relative to the incident light. When the light is polarized along the fiber axis, the intensities of all peaks are high ($\theta = 0°$) and they decrease to a minimum as the value of θ increases to 90°; that is, the polarized light is perpendicular to the fiber axis. The decrease in intensity of the Raman signal as a function of the orientation of the polarized laser beam relative to the fiber orientation depicts local alignment of the SWNT's in the fibers. Figure 5 shows a decrease in the intensity ratios of the D and TM bands with increase in orientation angle.

Introduction of nanotubes into silk leads to a shift in the D-band positions from 1294.8 to 1295.8 cm^{-1} (0.5% SWNT). There is an increase in the shift up to 2% nanotube loading (1299.8 cm^{-1}), after which further increases in the content of SWNT lead to a decrease in the D-band positions. When the nanotubes are incorporated into the silk, the bands are shifted toward higher frequencies, especially the lower frequency peaks (RBM). The shifts observed can be explained by the intercalation of the silk into the SWNT bundles. The silk exerts pressure on the individual tubes, thereby increasing the peak positions. Further, the quantity of silk intercalated between nanotubes could lead to further opening of the SWNT bundles, thereby enhancing the formation of nucleating sites to favor the crystallization process. These results may suggest that there is some reduced vibrational freedom of the silk polymer chains as a consequence of the intercalation of the silk matrix.

The presence of SWNT in the silk fibers and their orientation can be observed by TEM.

Analysis of a large number of fibers shows that tubes were aligned along the fiber axis, as previously reported for PAN fibers.[22] Figure 6 shows the TEM image of a broken reinforced fiber. The micrograph shows that the SWNTs are embedded in

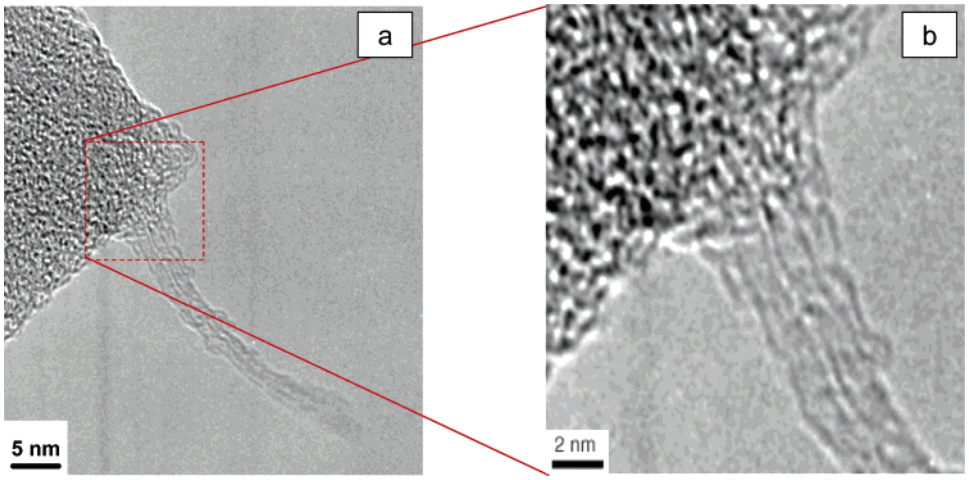

Figure 6. TEM micrographs of a SWNT reinforced silk fiber; (b) is a high-resolution TEM image of the area squared in (a) showing two single wall nanotubes protruding out of the silk fiber.

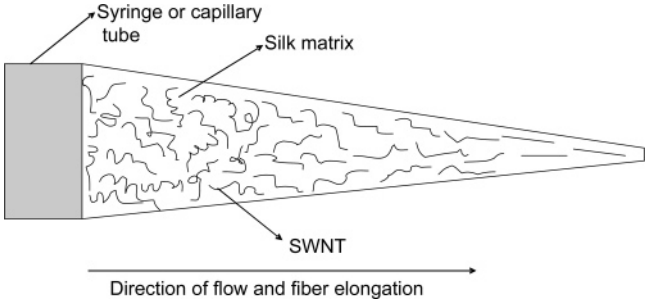

Figure 7. Schematic of flow and confinement mechanisms for preferred nanotubes orientation along fiber axis.

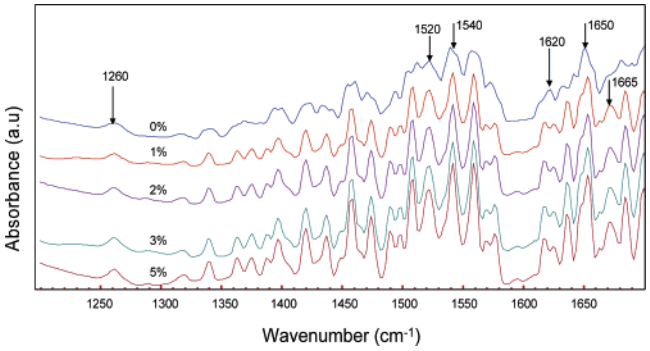

Figure 8. FTIR spectra of silk fibers: (a) as-spun, (b) 0.5% SWNT reinforced fiber, (c) 1% SWNT reinforced fiber, (d) 2% SWNT reinforced fiber, and (e) 5% SWNT reinforced fiber.

the silk fibers and not deposited on the surface during the electrospinning process. The high-resolution TEM image shows that the nanotubes are in the form of bundles and the average diameter of the nanotubes is ~1 nm.

The SWNTs may be aligned along the silk fiber axis by three mechanisms: (1) charge, (2) confinement, and (3) flow. Due to the large electrostatic fields used in the electrospinning process, a favored orientation of the SWNT along the fiber axis is achieved. As a result of the large aspect ratio of the nanotubes (L/d =1 μm/1 nm > 1000) and the nanoscale diameter of the electrospun silk fibers, a relative orientation is further attained due to confinement as there are not too many permissible orientations in the fiber that will allow movement of the nanotubes other than along the fiber axis. In addition, during the fiber formation stage in the electrospinning process, the silk matrix undergoes a drawing effect, which partially induces alignment of the SWNT along the flow direction (fiber axis). A coupling of these three mechanisms leads to a preferred alignment of SWNTs along the electrospun silk fibers.

Figure 7 shows a schematic of the flow and confinement induced alignment of SWNTs in a silk fiber.

The conformation of the aligned SWNT reinforced fiber was determined by FTIR. The absorption spectra were carried out on as-spun nanofibers and SWNT reinforced fibers at different nanotubes content levels. The spectra in Figure 8, show the fibers have random coils with strong absorption bands in the 1640−1690 cm^{-1} range (amide I), 1520−1570 cm^{-1} range (amide II), and an amide (III) band at 1260 cm^{-1}. The β-sheet bands of the amide I group are noticeable at 1620**,** 1632, and 1651 cm^{-1}, respectively.[44] The spectra indicate that there are no significant conformational differences between 0.5, 1, 2, and 5% SWNT reinforced fibers. There are no significant differences in the major bands; however, there are slight differences in peak intensities, which indicate changes in the amount or concentration.

An XDS 2000 WAXD was employed to determine the crystalline structure of the electrospun-unreinforced fibers and

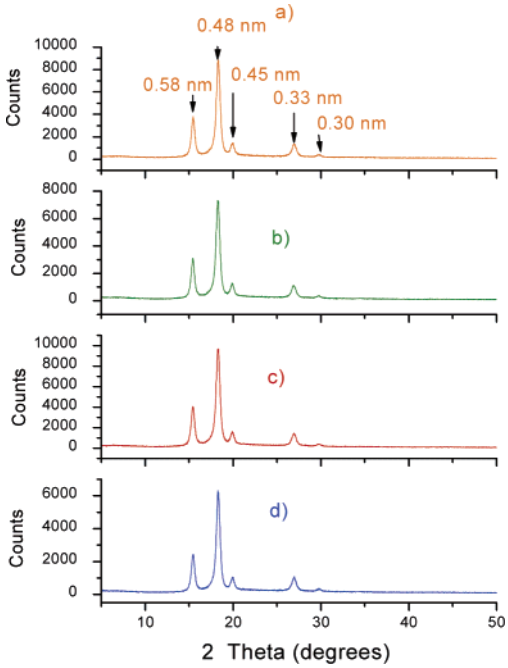

Figure 9. WAXD patterns of (a) as-spun silk, (b) 2% SWNT-silk fibers, (c) 1% SWNT-silk fiber, and (d) 0.5% SWNT reinforced silk fibers.

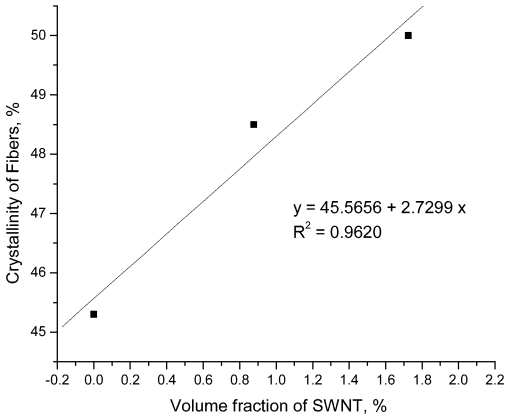

Figure 10. Crystallinity of reinforced silk fibers versus volume fraction of single wall carbon nanotubes.

SWNT reinforced fiber. Figure 9 shows the WAXD patterns of the nonreinforced and SWNT reinforced fiber. The SWNT reinforced fiber as well as unreinforced fiber were characterized by peaks at 15.4, 18.3, 19.9, 26.9, and 29.7° corresponding to silk (I) and silk (II) crystalline d spacings of 0.57(I), 0.49(II), 0.45(I), 0.33(I), and 0.30(I) nm, respectively. Figure 10 depicts the crystallinity of the SWNT reinforced fiber and unreinforced fiber (calculated by the method of Herman)[45] plotted against the volume fraction of SWNT in each fiber. The volume fraction was calculated from the mass fraction using the densities, ρ = 1500 kg/m^3 for SWNT and ρ = 1300 kg/m^3 for silk. It can be seen that there is a linear increase in crystallinity by reinforcing the silk fibers with 0.5−2% volume of SWNTs. This might suggest that SWNT may induce crystallization of silk.

The mechanical testing was conducted on aligned fibers, which were collected by a procedure developed in our laboratory as our previous research[5] has shown that random fibers do not possess satisfactory mechanical properties. The aligned fibers were carefully rolled into yarns with as few twists as possible and mounted on a paper sample holders (3 cm gauge length). Figure 11 shows the stress−strain curves for SWNT reinforced

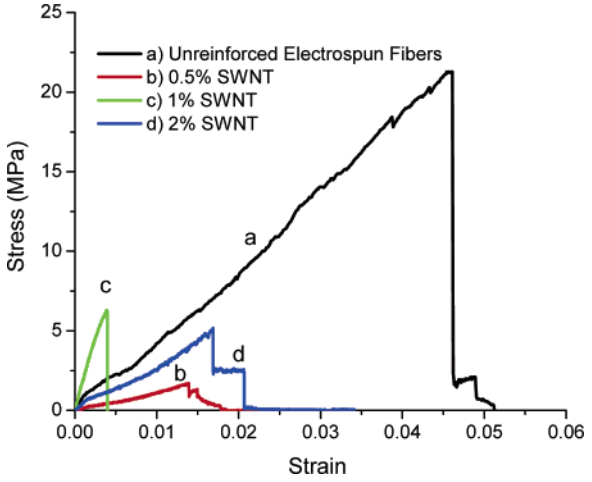

Figure 11. Typical stress−strain curves of aligned SWNT-reinforced and unreinforced fiber yarns.

Table 2. Mechanical Properties of Aligned Reinforced and Unreinforced Fiber Yarns[a]

type of fiber	initial Young's modulus (MPa)	max stress (MPa)	max strain (%)
aligned silk fibers	312 ± 193	19.1 ± 10.3	5.8 ± 1.7
0.5% SWNT reinforced	180 ± 108	2.84 ± 1.1	1.7 ± 0.3
1% SWNT reinforced	705 ± 698	7.4 ± 2.5	1.4 ± 0.8
2% SWNT reinforced	285 ± 112	3.7 ± 1.3	1.8 ± 0.5

[a] Values are means of 5 measurements.

fiber and unreinforced fiber, whereas Table 2 shows the averages of the mechanical properties.

The initial Young's modulus of the as-spun aligned fibers as calculated from the slope of the initial part of the stress−strain curve was 337 MPa at a breaking strain of 4.6%. The 0.5 and 2% SWNT reinforced fibers have a lower modulus in comparison with the aligned as-spun fibers. However, the 1% SWNT reinforced fibers show a much more promising result.

Reinforcing the fibers with 1% SWNT can lead to increases in the initial modulus in the range of 110−460%. We hypothesize that the lower mechanical properties of the 0.5 and 2% SWNT reinforced fibers are due to poor dispersion (distribution) and imperfect alignment of the nanotubes along the fiber axis within the nanofibers. Nanotube agglomerates can act as critical flaws decreasing the ultimate strain and strength of the fibers. Higher Young's modulus for the 1% SWNT reinforced fibers could be due to a more uniform distribution and alignment of SWNT along the nanofibers. This fiber also had the maximum diameter (Table 1).

Summary

In conclusion, we have demonstrated the feasibility of fabricating a nanocomposite fiber comprising *Bombyx mori* silk and SWNT through the electrospinning process. The conformation of the silk is conserved as shown by the FTIR results. The WAXD results show evidence of the possible nucleating effect of the SWNTs on the silk by the linear increase in crystallinity in the low volume fraction region. The mechanical properties of the SWNT-reinforced fibers show an increase in Young's modulus up to 460% in comparison with as-spun fibers, but at the expense of the strength and strain to failure.

Despite these promising results, it is well understood that the mechanical properties of the SWNT reinforced silk fibers are still not fully realized due to the nanotubes not being evenly distributed and aligned throughout the fibers. Further study is needed for improving the dispersion, achieving a uniform distribution of SWNTs in the electrospun fibers, having a better understanding of the SWNT−silk interactions, and identifying the optimal interfacial stress transfer conditions of the SWNT-silk composite in order to fully realize their properties and potential applications.

Acknowledgment. This work was supported by the Taiwan Textile Research Institute, Taiwan. This project is supported in part by the PA Nanotechnology Institute. SWNT were supplied by Dr. Peter Willis of NASA JPL. Special thanks to Dr. Christopher Li for advice and assistance with WAXD experiments. We thank Tim Kelly for his experimental assistance with FTIR and Raman spectroscopy. The NSF Grant numbers DMR-0116645 and BES-0216343 supported the Raman spectrometer and ESEM purchase, respectively. TEM work was carried out in the LRSM, University of Pennsylvania.

References and Notes

(1) Ogho, K.; Zhao, C.; Kobayashi, M.; Asakura, T. *Polymer* **2003**, *44*, 841−846.
(2) Matthews, J. A.; Wnek, G. E.; Simpson, D. G.; Bowlin, G. L. *Biomacromolecules* **2002**, *3*, 232−238.
(3) Doshi, J.; Reneker, D. *J. Electrost.* **1995**, *35*, 151−160.
(4) Zarkoob, S.; Reneker, D. H.; Eby, R. K.; Hudson, S. D.; Ertley, D.; Adams, W. W. *Polym. Preprints* **1998,** *39*, 244−245.
(5) Jin, H. J.; Fridrikh, S. V.; Rutledge, G. C.; Kaplan, D. L. *Biomacromolecules* **2002**, *3*, 1233−1239.
(6) Buchko, C. J.; Chen, L. C.; Shen, Y.;Marthin, D. C. *Polymer* **1999**, *40*, 7397−7407.
(7) Weixan, L. *J. Textile Res.* **2003**, *24*, 80−82.
(8) Ayutsede, J.; Gandhi, M.; Sukigara, S.; Micklus, M.; Chen, H.; Ko, F. *Polymer* **2005**, *46*, 1625−1634.
(9) Wang, M.; Jin, H.; Kaplan, D.; Rutledge, G. *Macromolecules* **2004**, *37*, 6856−6864.
(10) Lyons, J. M. *Melt-electrospinning of Thermoplastic Polymers: An Experimental and Theoretical Analysis*; Drexel University: Philadelphia, 2004.
(11) Pedicini, A.; Farris, R. *J. Polym.* **2003**, *44*, 6857−6862.
(12) Anderson, J. P.; McGrath, K.; Kaplan, D. In *Protein-based materials*; Birkhauser: Basel, 1997; pp 371−423.
(13) Vollrath, F.; Knight, D. *Nature* **2001**, *6828*, 541−548.
(14) Shao, Z.; Vollrath, F. *Nature* **2002**, *418*, 741.
(15) Lau, K.; Chipara, M.; Ling, H.; Hui, D. *Composites: Part B* **2004**, *35*, 95−101.
(16) Che, G.; Lakshmi, B. B.; Fisher, E. R.; Martin, C. R. *Nature* **1998**, *393*, 346−349.
(17) Frank, S.; Poncharal, P.; Wang, Z. L.; De Heer, W. A. *Science* **1998**, *280*, 1744−1746.
(18) Planeix, J. M.; Coustel, N.; Coq, B.; Brotons, V.; Kumbhar, P. S.; Dutartre, R.; Geneste, P.; Bernier, P.; Ajayan, P. M. *J. Am. Chem. Soc.* **1994**, *116*, 7935−7936.
(19) Panhuis, M. *Chem. Biol.* **2003**, *10*, 897−898.
(20) Minoura, N.; Aiba, S.; Gotoh, Y.; Tsukadaa, M.; Imai, Y. J. *Biomed. Mater. Res.* **1995**, *29*, 1215−1221.
(21) Chiarini, A.; Petrini, P.; Bozzini, S.; Dal Pra, I.; Armato, U. *Biomaterials* **2003**, *24*, 789−799.
(22) Sugihara, A.; Sugiura, K.; Morita, H.; Ninagawa, T.; Tabouchi, K.; Tobe, R.; Izumiya, M.; Horio, T.; Abraham, N. G.; Ikehara, S. *Proc. Soc. Exp. Biol. Med.* **2000**, *225*, 58−64.
(23) Khil, M. S.; Cha, D. I.; Kim, H. Y.; Kim, I. S.; Bhattarai, N. *J. Biomed. Mater. Res. B. Appl. Biomater.* **2003**, *67*, 675−679.
(24) Sano, M.; Kamino, A.; Okamura, J.; Shinkai, S. *Science* **2001**, *293*, 1299−1301.
(25) Riggs, J. E.; Gou, Z.; Carroll, D. L.; Sun, Y. P. *J. Am. Chem. Soc.* **2000**, *122*, 5879−5880.
(26) Jiang, L.; Gao, L.; Sun, J. *J. Colloid Interface Sci.* **2003**, *260*, 89−94.
(27) Chen, J.; Rao, A. M.; Lyuksyutov, S.; Itkis, M. E.; Hamon, M. A.; Hu, H.; Cohn, R. W.; Eklund, P. C.; Colbert, D. T.; Smalley, R. E.; Haddon, R. C. *J. Phys. Chem.* **2001**, *105*, 2525−2528.

(28) O'Connell, M. J.; Boul, P.; Ericson, L.; Huffman, C.; Wang, Y.; Haroz, E.; Kuper, C.; Tour, J.; Ausman, K. D.; Smalley, R. E. *Chem. Phys. Lett.* **2001**, *342*, 265−271.
(29) Li, D.; Wang, H.; Zhu, J.; Wang, X.; Lu, L.; Yang, X. *Mater. Sci. Lett.* **2003**, *22*, 253−255.
(30) Sen, R.; Zhao, B.; Perea, D.; Itkis, M.; Hu, H.; Love, J.; Bekyarova, E.; Haddon, R. *Nano Lett.* **2004**, *4*, 459−464.
(31) Qian, D.; Dickey, E. C.; Andrews, R.; Rantell, T. *App. Phys. Lett.* **2000**, *76*, 2868−2870.
(32) Wagner, H. D.; Lourie, O.; Feldman, Y.; Tenne, R. *App. Phys. Lett.* **1998**, *72*, 188−190.
(33) Andrews, R.; Jacques, D.; Rao, A. M.; Rantell, T.; Derbyshire, F.; Chen, Y.; Chen, J.; Haddon, R. C. *App. Phys. Lett.* **1999**, *75*, 1329−1331.
(34) Ko, F.; Gogotsi, Y.; Ali, A.; Naguib, N.; Ye, H.; Yang, G.; Li, C.; Willis P. *Adv. Mater.* **2003**, *15*, 1161−1165.
(35) Ye, H.; Lam, H.; Titchenal, N.; Gogotsi, Y.; Ko, F. *App. Phys. Lett.* **2004**, *85*, 1775−1777.
(36) Balavione, F.; Schultz, P.; Richard, C.; Mallouh, V.; Ebbesen, T. W.; Mioskowski, C. *Angew. Chem., Int. Ed. Engl.* **1999**, *38*, 1912−1915.
(37) Bronikowski, M.; Willis, P. A.; Colbert, D.; Smith, K. A.; Smalley, R. E. *J. Vac. Sci. Technol. (A)* **2001,** *19*, 1800.
(38) Sukigara, S.; Gandhi, M.; Ayutsede, J.; Micklus, M.; Ko, F. *Polymer* **2003**, *44*, 5721−5727.
(39) Lam, H. Electrospinning of single wall carbon nanotube reinforced aligned fibrils and yarns. Ph.D. Thesis, Drexel University, 2004.
(40) Dresselhaus, M. S.; Pimenta, M. A. *Raman Scattering in Carbon Materials, in Analytical Applications of Raman Spectroscopy*; Pelletier, M. J., Ed.; Blackwell Science: London, 1999; pp 265−271.
(41) Souza-Filho, A. G.; Jorio, A.; Samsonidze, G.; Dresselhaus, G.; Saito, R.; Dresselhaus, M. S. *Nanotechnology* **2003**, *14*, 1130−1139.
(42) Tan, P. H.; Dimovski, S.; Gogotsi, Y. *Philos. Trans. R. Soc. London A* **2004**, *362*, 2289−2310.
(43) Osswald, S.; Flahaut, E.; Ye, H.; Gogotsi, Y. *Chem. Phys. Lett.* **2005**, *402*, 422−427.
(44) Um, I. C.; Kweon, H. Y.; Lee, K. G.; Park, Y. H. *Int. J. Biol. Macromol.* **2003**, *33*, 203-213.
(45) Weidinger, A.; Hermans, P. H. *Makromol. Chem.* **1961**, 50, 98−115.

BM0505888